

Basal crevasses and associated surface crevassing on the Larsen C ice shelf, Antarctica, and their role in ice-shelf instability

Daniel McGRATH,¹ Konrad STEFFEN,¹ Ted SCAMBOS,² Harihar RAJARAM,³
Gino CASASSA,⁴ Jose Luis RODRIGUEZ LAGOS⁴

¹*Cooperative Institute for Research in Environmental Sciences (CIRES), University of Colorado at Boulder, Boulder, CO, USA*
E-mail: daniel.mcgrath@colorado.edu

²*National Snow and Ice Data Center (NSIDC), CIRES, University of Colorado at Boulder, Boulder, CO, USA*

³*Department of Civil Engineering, University of Colorado at Boulder, Boulder, CO, USA*

⁴*Centro de Estudios Científicos, Valdivia, Chile*

ABSTRACT. We identify a series of basal crevasses along a 31 km transect across the northern sector of the Larsen C ice shelf, Antarctica, using in situ ground-penetrating radar. The basal crevasses propagate from a region of multiple, shallow basal fractures to form widely spaced (0.5–2.0 km) but deeply incised (70–134 m) features. Surface troughs, observed in visible imagery, exist above the basal crevasses as the ice vertically shears to reach hydrostatic equilibrium, while widespread surface crevassing occurs along the crests and on the flanks of the undulations, primarily aligned with the topography. We suggest, based on the location of the surface crevasses and the along-flow evolution of the basal crevasses, that the former are induced by a bending stress created by gradients in hydrostatic forces. Using a linear elastic fracture mechanics model, we investigate the sensitivity of basal crevasse propagation to observed trends of ice-shelf thinning and acceleration. Basal crevasses are large-scale structural weaknesses that can both control meltwater ponding and induce surface crevassing. Together, these features may represent an important mechanism in both past and future ice-shelf disintegration events on the Antarctic Peninsula.

INTRODUCTION

Over 28 000 km² of floating ice shelves have disintegrated along the Antarctic Peninsula (AP) over the past three decades, punctuated by the catastrophic break-up of Larsen A in 1995 and Larsen B in 2002 (Cook and Vaughan, 2010). The final collapse of these ice shelves appears to be directly tied to increased meltwater production and surface crevasse hydrofracture, rendering the ice shelf into a series of unstable narrow blocks, capable of rapid disintegration (Scambos and others, 2000, 2003; MacAyeal and others, 2003). However, the rapid collapse masks the slow preconditioning of the shelves in the preceding years, processes that make them increasingly susceptible to this style of break-up. The preconditioning has been primarily driven by a 2.5°C atmospheric warming along the AP since 1950, which has, at least partially, been driven by changes in the Southern Annular Mode index. The result has been increased advection of warm, maritime air from lower latitudes towards the AP (Vaughan and others, 2003; Orr and others, 2004). Strengthening of the westerly winds increases the passage of this air mass over the peninsula, where it is further warmed by the föhn effect and certainly contributed to the increased surface melt on Larsen B prior to its break-up (Orr and others, 2004, 2008; Van den Broeke, 2005). Increased surface melt has driven firn densification and the formation of ice layers, eventually allowing melt ponds to be supported on the shelf surface (Scambos and others, 2000, 2003; Fahnestock and others, 2002; Van den Broeke, 2005; Vaughan, 2006; Holland and others, 2011).

Increased basal melting has been shown to be a key preconditioning process for ice-shelf disintegration as well, primarily by thinning the ice shelf and thus reducing resistive stresses at lateral shear margins and ice rises (Glasser and Scambos, 2008). However, unlike the

Amundsen–Bellingshausen Sea sector, where the incursion of warm, Circumpolar Deep Water onto the continental shelf has been well documented and has been shown to drive the high basal melt rates beneath the Pine Island Glacier ice shelf, the ice shelves in the Weddell Sea sector are protected from this water mass (Jacobs and others, 2011). Weddell Deep Water has shown substantial decadal variability in temperature and salinity properties, yet no sustained long-term trends have been observed (Robertson and others, 2002; Fahrbach and others, 2004). Basal melting (and refreezing) is still believed to substantially modify the ice shelves in the Weddell Sea sector, although limited oceanographic measurements prevent a complete understanding of the extent and magnitude of these processes (Shepherd and others, 2003; Nicholls and others, 2004; Glasser and Scambos, 2008; Holland and others, 2009; Khazendar and others, 2011).

Crevasse hydrofracture, the process by which water-filled surface crevasses propagate downwards, possibly through the entire ice thickness, has been shown to be a key mechanism in polar glaciology (Weertman, 1973; Van der Veen, 1998a; Zwally and others, 2002; Das and others, 2008). On ice shelves, surface crevasses often form near the ice-shelf grounding line, along shear margins, or at the ice-shelf front due to bending stresses (Scambos and others, 2003, 2009). Crevasses formed in upstream areas are commonly advected into the floating portion of the ice shelf as well. The filling of surface crevasses with meltwater increases the stress intensity at the crevasse tip, which, if it exceeds the fracture toughness of ice, allows the crevasse to propagate further downwards (Van der Veen, 1998a). Continued crevasse propagation is dependent on having sufficient meltwater volume to maintain a high level in the crevasse as it propagates downward. Thus, the ability of an ice shelf to support surface melt ponds is one harbinger of

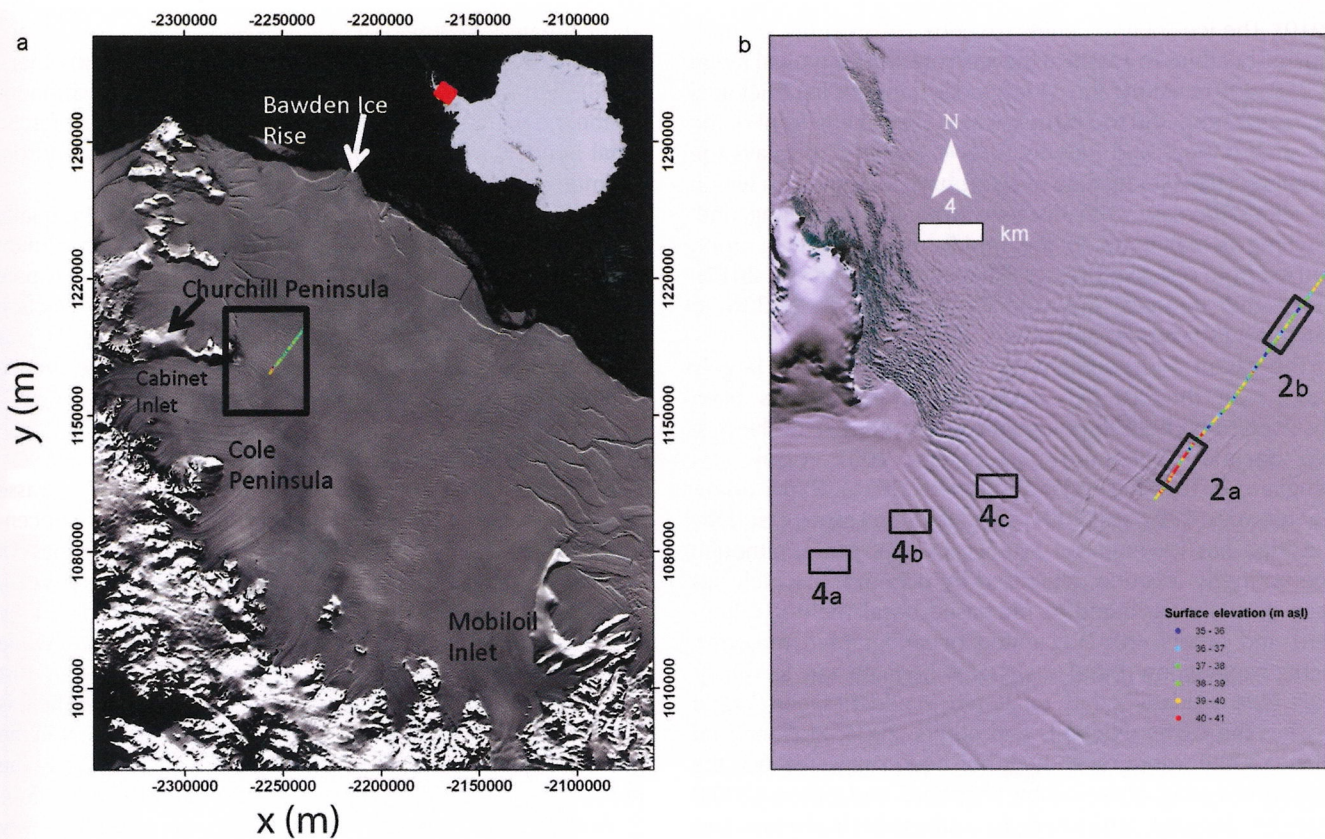


Fig. 1. (a) Subsection of Moderate Resolution Imaging Spectroradiometer (MODIS) Mosaic of Antarctica (MOA) detailing the Larsen C ice shelf with prominent geographic features labeled (Haran and others, 2005). Radar transect is shown as colored line corresponding to surface elevations from kinematic GPS. Black box indicates location of (b). Inset: Location of MODIS image on the Antarctic Peninsula. Coordinates are polar stereographic (at 71° S secant plane, 0° meridian, World Geodetic System 1984 (WGS84) ellipsoid) where x is easting and y is northing. (b) Landsat Image Mosaic of Antarctica (LIMA) image of the edge of Churchill Peninsula with the surface undulations visible. Black boxes indicate location of radar profiles shown in Figure 2 and high-resolution imagery shown in Figure 4.

collapse (Scambos and others, 2003), although low confining stress (longitudinal or transverse) is also necessary, in order to permit crevasse deepening by hydrofracture (Cook and Vaughan, 2010).

While the role of surface crevasse propagation has received significant attention, the role of basal crevasses, which form at the shelf bottom and extend upwards into the ice, has received less attention. Airborne radar surveys have identified large hyperbolic radar returns, interpreted as basal crevasses, within the Ross (Jezek and others, 1979), Larsen (Swithinbank, 1977) and Riiser-Larsen ice shelves (Orheim, 1982). Weertman (1973, 1980) suggested that the height of a single basal crevasse, h , on a free-floating ice shelf of thickness H is

$$h = \frac{\pi H}{4}. \quad (1)$$

Both surface and basal crevasses are rarely found individually, and the presence of multiple crevasses in close proximity reduces the overall stress field, thus limiting the penetration height to one-half the ice thickness (Weertman, 1980). Still, field measurements of basal crevasse heights were found to be significantly smaller than predicted by Eqn (1). Jezek (1984) hypothesized that the embayed walls and ice rises constraining the ice shelf resulted in a compressive back-stress that resisted both ice flow and crevasse propagation. Rist (1996), Rist and others (1996, 2002) and Van der Veen (1998b) extended the theoretical analysis of basal

crevasse propagation by utilizing a linear elastic fracture mechanics (LEFM) approach. By integrating the stresses along the length of the crevasse, they calculate the stress intensity factor at the crevasse tip, K_I , which is compared to a critical value, K_{IC} , the fracture toughness of the ice, to determine the height to which a crevasse will propagate (Rist and others, 2002).

We present in situ ground-based radar observations of basal crevasses along a 31 km transect across the northern section of the Larsen C ice shelf, Antarctica. We describe the basal crevasse properties and how they evolve as they are advected towards the calving front. We present high-resolution satellite imagery detailing the development of surface crevassing primarily aligned with the crests of the surface undulations. We model the theoretical penetration height of a basal crevasse at its point of formation, based on the LEFM model of Van der Veen (1998b) and investigate the sensitivity of penetration height to observed changes. We conclude with a discussion of the possible contribution of these features to ice-shelf instability in light of observations of change in this sector of the Larsen C ice shelf.

STUDY SITE

Larsen C is the largest remaining ice shelf on the AP, consisting of $>50\,000$ km² of floating ice, which is fed from 12 major outlet glaciers flowing off the mountainous spine of the AP (Fig. 1a; Glasser and others, 2009; Cook and Vaughan,

2010). The ice-shelf thickness exceeds 700 m at the grounding line but thins to 150 m at the ice front, with a typical range of 250–400 m. Along the 31 km radar transect, ice thickness decreases from 300 to 280 m towards the calving front of the ice shelf (Griggs and Bamber, 2009). Larsen C displays the characteristic velocity field of an embayed ice shelf, in which velocities increase with distance from the grounding line, reaching a maximum in the middle of the calving front, furthest from resistive stresses (Khazendar and others, 2011). Along this transect, ice velocity increases from 328 to 355 m a⁻¹ (Khazendar and others, 2011).

The extent and geometry of Larsen C has been largely stable over the last five decades, although it has been observed to be both thinning and accelerating over the past two decades (Shepherd and others, 2003; Cook and Vaughan, 2010; Khazendar and others, 2011). Radar altimetry between 1992 and 2001 found that the Larsen C surface elevation has lowered, on average by 0.08 m a⁻¹, although one northerly location decreased by 0.27 m a⁻¹, which has been partially attributed to increased basal melting (Shepherd and others, 2003). Limited oceanographic measurements suggest low basal melt rates beneath the ice shelf, with little evidence that unaltered Weddell Deep Water reaches the cavity (Nicholls and others, 2004; Holland and others, 2009). More recently, it has been suggested that the surface lowering observed by Shepherd and others (2003) may be largely attributed to atmospheric-driven firn densification (Holland and others, 2011). Khazendar and others (2011) found that the northern sector of the ice shelf accelerated by 80 m a⁻¹ or 15% between 2000 and 2006, and a further 6–8% between 2006 and 2008 in Cabinet Inlet, possibly due to a reduction in back-stress from the Bawden Ice Rise and/or the erosion of marine ice formerly suturing neighboring flowbands together.

METHODS

Data acquisition and processing

Radar surveys were conducted with a Malå Geoscience ground-based pulse radar system (CU-II control unit) with a 25 MHz (~6.8 m wavelength in ice) antenna pulled behind a snowmobile traveling at an average of 4.5 m s⁻¹. We recorded at 1024 16-bit samples per trace and each trace lasted ~4000 ns. A 16-fold stack was applied during recording. To improve the signal-to-noise ratio of the radar data, the mean waveform was removed from all profiles and a dewow filter was applied to remove direct-current bias and low-frequency drift. The measured two-way travel time was converted to depth assuming a mean radar velocity of 0.173 m ns⁻¹, which incorporates a linear decrease from 0.190 m ns⁻¹ at the surface (in the firn) to 0.168 m ns⁻¹ at the depth of the firn/ice transition. This depth was determined from the RACMO2 regional atmospheric climate model (personal communication from M. van den Broeke, 2011). Radargrams are presented as unmigrated to emphasize the reflection hyperbolas within the ice column.

Kinematic GPS data were collected simultaneously using a Trimble GeoXT unit mounted to the radar sledge with a ±1.03 m horizontal precision and ±1.86 m vertical precision. Position data were collected relative to the World Geodetic System 1984 (WGS84) ellipsoid and were corrected to heights above mean sea level (m.s.l.) using the EIGEN-GL04C geoid, which combines Gravity Recovery

and Climate Experiment (GRACE) satellite data and surface gravity data from altimetry and gravimetry (Förste and others, 2008). Surface elevations were then corrected for variations in the tidal amplitude (±1 m) using the Circum-Antarctic Tidal Simulation version 2008a (CATS2008a), updated from Padman and others (2002).

The ice-shelf/ocean interface reflection was manually delineated along each profile by following the maximum amplitude in the radar waveform near the approximate interface. This was only done where the interface reflection was strong and easily determined. The ice thickness, H , was then calculated by taking the difference between the surface height, z , and the identified ice/ocean interface.

Basal crevasse propagation model

Based on a LFM approach, an individual basal crevasse should penetrate to a given height where the stress concentration near the crevasse tip equals the fracture toughness of the ice, K_{IC} (Rist, 1996; Rist and others, 1996; Van der Veen, 1998b). The stress intensity factor, K_I , is estimated by integrating the stress along the length of the fracture, while the fracture toughness of nonporous ice, measured by Rist and others (2002) on an ice core from the Ronne Ice Shelf, is 0.155 MPa m^{1/2}. There is some historical evidence that in the presence of salt water, the fracture toughness may be reduced by a factor of up to 3 (Johnston and Parker, 1957).

According to Van der Veen (1998b), the stress intensity factor at the crevasse tip may be described as

$$K_I = \int_0^h \frac{2\sigma_n(z)}{\sqrt{\pi h}} G(\gamma, \lambda) dz, \quad (2)$$

where h is the crevasse height, σ_n is the net longitudinal stress, H is the ice thickness, z is the height within the ice column ($z=0$ at base) and G is a function of $\lambda=h/H$ and $\gamma=z/h$. The net longitudinal stress, σ_n , is the integral of the lithostatic stress, acting to close the crevasse, whereas sea-water pressure in the basal crevasse and the tensile spreading stress, R_{xx} , act to further open the crevasse (Van der Veen, 1998b). We extract longitudinal strain rates from interferometric synthetic aperture radar (InSAR)-derived surface velocities along the transect (Khazendar and others, 2011; personal communication from E. Rignot, 2011). The tensile spreading stress is related to the stretching rate through the flow rate factor, B , which has a strong dependence on temperature (Van der Veen and Whillans, 1989). We calculate a parabolic temperature profile within the ice column assuming basal melting, with the surface constrained by in situ automatic weather station mean annual temperature (−12°C) and an assumed basal temperature at the approximate freezing point of sea water (−2°C; Sandhäger and others, 2005). Given the observed geometry of the basal crevasses (i.e. spacing \gg height), we model the basal crevasses as individual features. For a more complete discussion of this model see Van der Veen (1998a,b).

RESULTS

Radar survey

Twenty-seven basal crevasses, with an average spacing of 1.2 km, are identified along a 31 km transect aligned with the flow direction of the ice shelf downstream of Cabinet Inlet. Basal crevasses are identified by strong hyperbolic reflections within the ice column (Fig. 2, black arrows) and

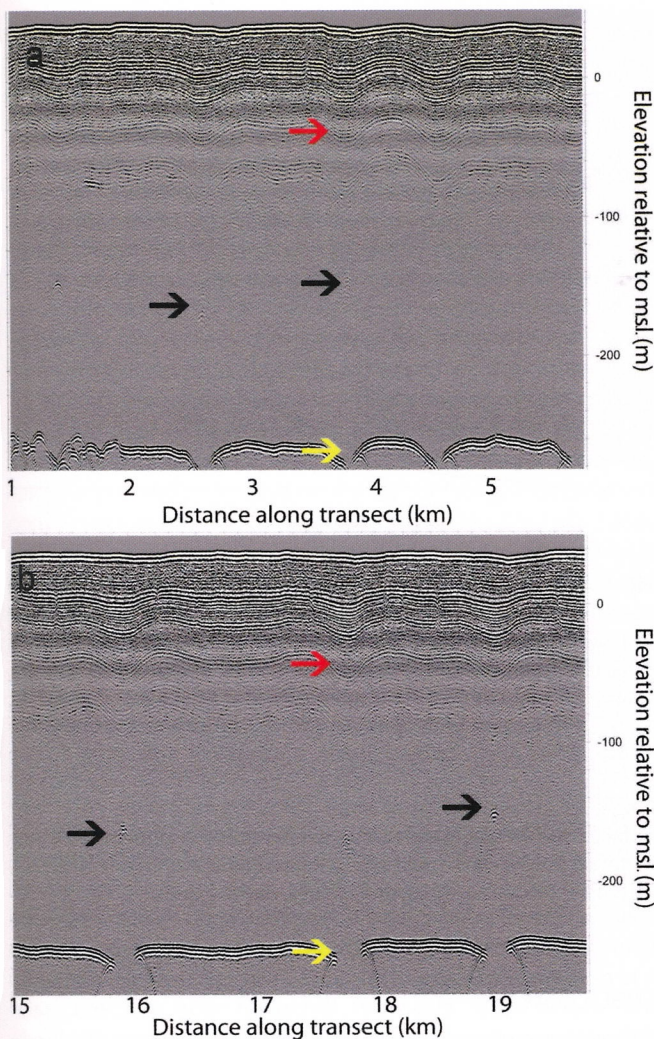


Fig. 2. 25 MHz radar profiles from two sections of the 31 km transect. (a) Basal crevasses (black arrows) emerge from a region of highly fractured basal ice. Hyperbolas from the bottom corners overlap (yellow arrow), preventing crevasse width from being known in this section. Firn layers slump above the basal crevasses in response to hydrostatic equilibrium (red arrow). (b) Arrows the same as (a). Both absolute crevasse height and height as a percentage of ice thickness are smaller in this section of the profile.

two, nearly symmetric hyperbolas at the bottom corners of the crevasse (Fig. 2, yellow arrows). The underside of the ice shelf is highly fractured in the initial 2 km of the transect; however, a smooth basal surface exists along the remainder of the transect (Fig. 2). Crevasse spacing ranges from 0.5 to 2.0 km and does not systematically vary along the length of the transect. Penetration height of the basal crevasses is greatest near the origin, where they extend 120–134 m into the ice column (Fig. 3). Height subsequently decreases along the length of the profile, decreasing by ~ 40 m in the first 15 km while remaining nearly constant over the remaining ~ 15 km (Fig. 3). In addition to a decrease in absolute height, the relative penetration height (as a function of ice thickness) also decreases from $\sim 40\%$ to 25% . Initially, the bottom width of the basal crevasses is quite narrow (20–70 m) and, at times, difficult to determine due to the overlap of the two hyperbolas that originate from the bottom corners of the crevasse (Fig. 2a, yellow arrow). The opening width of the basal crevasses increases along the

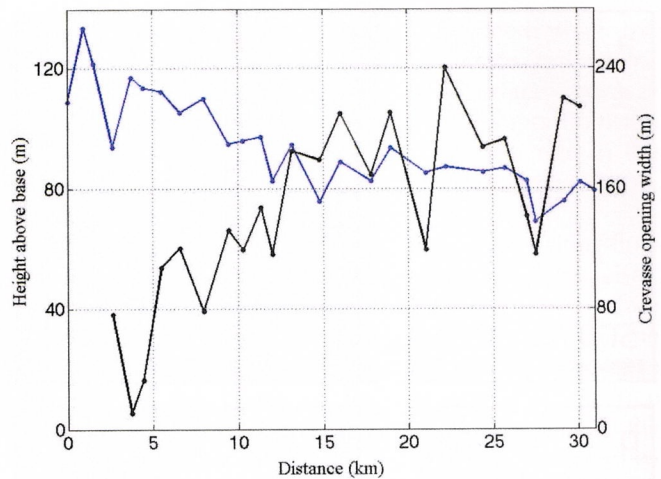


Fig. 3. Observed crevasse penetration height (blue; left y-axis) and crevasse opening width (black; right y-axis) along radar transect.

length of the transect, opening ~ 100 m in the first 15 km, while ranging between 150 and 240 m over the remaining ~ 15 km (Fig. 3, black line). The surface undulations have an amplitude of 3–4 m, although the amplitude of these features is likely much larger proximal to Churchill Peninsula, as the radar transect was conducted near the edge of the features. Internal layering within the firn shows significant downwarping of 11–18 m above the basal crevasses, with deeper layers showing greater downwarping (Fig. 2, red arrows).

Satellite imagery

Surface undulations on the ice shelf are easily identified in both Moderate Resolution Imaging Spectroradiometer (MODIS; 250 m) and Landsat (15 m) imagery as a series of parallel alternating dark and light bands (Fig. 1). In total, 102 undulations, with the troughs aligned with the basal crevasses, are observed along a 155 km flowline transect. High-resolution commercial visible imagery (GeoEye; 1.65 m resolution) clearly shows a lack of surface crevassing upstream of the origin of the basal crevasses (Fig. 4a). Surface crevassing, first observed as narrow (1–5 m) bridged features, is apparent where the first surface undulations are observed (Fig. 4b). The surface crevasses become increasingly abundant and well defined in the along-flow direction, reaching widths of 8–24 m, while remaining primarily aligned with the crests of the surface undulations (Fig. 4c).

MODEL

We apply the model to examine basal crevasse propagation at the point of formation and do not intend to model propagation of pre-existing crevasses/undulations to changing conditions. Using reasonable parameters at the origin of the basal crevasses (ice thickness (H) = 300 m; surface temperature (T_s) = -12°C ; stretching rate (ϵ_{xx}) = 0.002 a^{-1}), the model predicts that if an initial basal fracture or flaw of ~ 2 m is present, the basal crevasse will propagate to a height of 128 m (Fig. 5). This agrees well with radar observations of basal crevasse heights of 120–134 m near the beginning of the radar transect. The primary parameters that affect crevasse propagation are the stretching rate, ice thickness

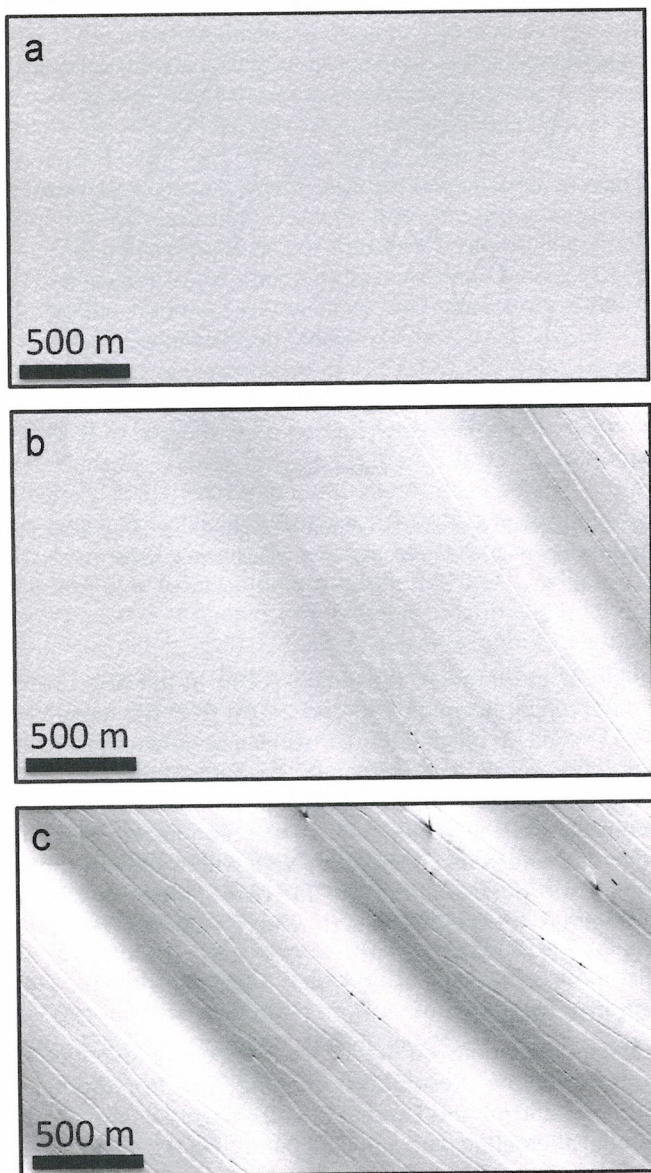


Fig. 4. GeoEye high-resolution (1.65 m) visible imagery of (a) smooth ice-shelf surface upstream of surface crevasses, (b) initial surface undulations and development of surface crevasses and (c) fully developed surface crevasses aligned with surface crests. Image locations are shown in Figure 1b. Copyright GeoEye Inc., 2011, provided by the US National Geospatial-Intelligence Agency (NGA) Commercial Satellite Imagery Program.

and surface temperature and hence we explore the sensitivity of basal crevasse propagation considering possible future changes affecting these parameters (Van der Veen, 1998b). An increase in the stretching rate results in the largest increase in crevasse propagation height, as an increase from 0.002 a^{-1} to 0.003 a^{-1} or 0.004 a^{-1} increases propagation height to ~ 166 and $\sim 205 \text{ m}$ (Fig. 5). For the subsequent three configurations, the stretching rate is held constant at 0.002 a^{-1} . The flow rate factor, which relates deviatoric stress and strain rate in Glen's flow law, is temperature-dependent, and hence if the mean surface temperature warms to -9°C , basal crevasse height decreases to 106 m (Fig. 5). If the ice shelf thins to 270 m , due to either increased basal or surface melting with subsequent runoff, basal crevasses will be able to propagate to a height of $\sim 133 \text{ m}$, due to a reduction in the overlying lithostatic stress (Fig. 5).

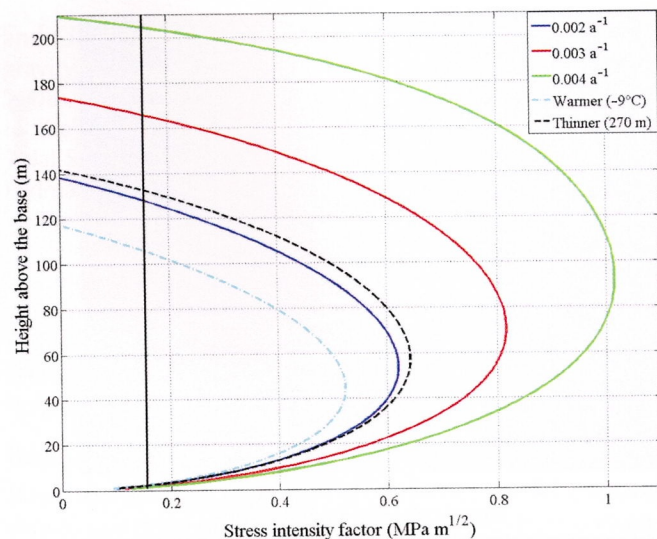


Fig. 5. Stress intensity factor, K_I , as a function of height above the ice-shelf base. Initial flaws that exceed the fracture toughness of the ice, defined as the critical stress intensity factor ($K_{IC} = 0.155 \text{ MPa m}^{1/2}$; black vertical line) will propagate to the height where $K_I = K_{IC}$. Using present-day ice-shelf parameters ($H = 300 \text{ m}$; $T_S = -12^\circ\text{C}$; $\varepsilon_{xx} = 0.002 \text{ a}^{-1}$), an initial flaw of 2 m will propagate to a height of 128 m (blue line). Increasing the longitudinal stretching rate to 0.003 a^{-1} (red solid line) or 0.004 a^{-1} (green solid line) increases the height of penetration. A warmer surface temperature ($T_S = -9^\circ\text{C}$) reduces the height, due to the temperature-dependent flow rate factor (cyan dot-dash line), while thinning the ice shelf ($H = 270 \text{ m}$) increases crevasse propagation (black dashed line).

DISCUSSION

We observe a series of basal crevasses, perpendicular to flow, in the northern sector of the Larsen C ice shelf. It is likely that these crevasses form as the outflow from Cabinet Inlet rounds Cape Alexander on Churchill Peninsula and subsequently accelerates and thins as it joins the main body of the ice shelf. Elevated stress in this region drives the formation and propagation of basal crevasses, which are subsequently advected towards the calving front, resulting in the series of surface undulations visible to the calving front (Fig. 1a). Assuming that this is indeed the location and mechanism by which the basal crevasses form, this process has occurred for a minimum of ~ 400 years (based on the 155 km length of surface undulations and current surface velocity). The initial section of the radar transect shows numerous shallow and overlapping hyperbolae, indicative of a large number of small fractures (Fig. 2). It is unclear how the evenly spaced, but not annually formed (i.e. spacing $>$ annual velocity), basal crevasses observed along the length of the transect emerge from this highly fractured underside, and in particular, why certain fractures preferentially propagate. Regardless, this region of highly fractured basal ice certainly provides the necessary minimum flow size ($\sim 2 \text{ m}$) for crevasse propagation (Fig. 5; Van der Veen, 1998b).

A. Luckman and others (unpublished information) find a series of basal crevasses, similar in nature to these observed near Churchill Peninsula, but in a more southerly sector of Larsen C. These crevasses show the same quasi-periodic nature, with an average spacing of $\sim 1 \text{ km}$, and form near the grounding line of Trail Inlet and similarly persist to the calving front. Observations of comparable crevasse heights and subsequently formed surface troughs give credence to

the idea that basal crevasses are an abundant feature of the Larsen C ice shelf and not isolated to our study region. Thus, understanding their evolution is key to understanding the mechanical structure and stability of Larsen C.

Two distinct patterns emerge in the basal crevasse geometries along the transect that provide insight into the processes affecting their evolution (Fig. 3). Penetration height of the basal crevasses decreases rapidly over the first 15 km, while crevasse-opening width increases substantially over this length (Fig. 3). Both parameters show large variability but no net change over the final ~ 15 km of the transect. We suggest that the observed evolution towards wider and shallower features is likely the result of bending stresses, possibly in conjunction with marine ice accretion along the upper walls and apex of the basal crevasses. Another possibility for this evolution includes a melt-driven convective cycle within the basal crevasse, with basal melting along the lower walls and marine ice accretion at the top (Khazendar and Jenkins, 2003). We suggest, for multiple reasons, that bending stresses, expressed as an alternating pattern of compression and extension, are the dominant mechanism for the observed evolution in basal crevasse geometry.

In the simplest sense, if the ice shelf is thought of as an unconfined slab, floating in equilibrium within the ocean, the freeboard height is equivalent to the balance between the downward-pointing lithostatic force of the ice column and the upward-pointing buoyancy force. If the slab is perturbed by the addition of basal crevasses, there will be reduced buoyancy above these features, which can be thought of as a downward negative force acting on the ice-shelf surface aligned with these features. Thus, following the formation of a basal crevasse near Churchill Peninsula, the firn and ice above the crevasse vertically shears in an attempt to reach hydrostatic equilibrium, as seen by the downwarped firn layers above the basal crevasses in the radargrams (Fig. 2). However, this ice is not an isolated column and is therefore partially supported by beam stresses from the neighboring ice of greater thickness (and hence greater buoyancy). Thus, the vertical shear above two neighboring basal crevasses induces a bending stress across the surface crest that separates the basal crevasses and results in the abundant surface crevassing observed in Figure 4c. This process is repeated for every basal crevasse and surface crest pair, creating alternating regions of compression in the surface troughs and extension over the surface crests, with the inverse of these forces on the underside of the shelf. This in turn explains the expansion of the basal crevasse opening width in the along-flow direction (Fig. 3).

Bending stresses have been observed in other contexts on floating ice shelves as well. Casassa and Whillans (1994) model the decay of surface topography on the Ross Ice Shelf and find that sinking regions of the ice shelf have compression at the ice surface and extension at the ice-shelf base, while the opposite stress pattern is present in neighboring regions. Similarly, Jenkins and others (2006) hypothesize, based on measured strain rates, that vertical shear stresses exist within the ice shelf soon after flotation at the grounding line, to balance the gravitational forces as the ice shelf attempts to reach its equilibrium level. These stresses induce compression at the ice-shelf surface and extension at the shelf bottom, in agreement with Casassa and Whillans (1994). Further, an outward bending stress exists at the calving front of ice shelves, as the hydrostatic

pressure increases more rapidly with depth than the lithostatic stress in the ice column (Scambos and others, 2009). This extensional stress drives surface crevasse formation (at a distance of $\sim 0.7 \times$ ice thickness from the ice front) and may have played an important role in the break-up of the Wilkins Ice Shelf (Braun and others, 2009; Scambos and others, 2009).

The evolution of surface crevassing in the along-flow direction provides direct visual support for this mechanism. Upstream of the basal crevasses, no surface crevasses are observed (Fig. 4a), but following the initial formation of the basal crevasses, numerous but narrow surface crevasses are observed at the crests of the low-amplitude surface undulations (Fig. 4b). These crevasses first form due to the extensional bending stresses at the crest surface invoked by vertical shear forces as the ice shelf attempts to reach hydrostatic equilibrium. Further along flow, surface crevassing is well defined, abundant and wide (8–24 m in width; Fig. 4c) and found along the crests and upper flanks of the large-amplitude surface undulations. Thus, the increased number and size of the surface crevasses correspond to a similar increase in undulation amplitude, indicative of an increase in vertical shear and extensional bending stresses. Once the ice shelf reaches approximate hydrostatic equilibrium, no further development of either surface crevasses or undulation amplitude occurs, suggesting that both the vertical shear and extensional bending stresses are substantially reduced. This is supported by the relative stability of basal crevasse height and opening width along the final 15 km of the radar transect, following rapid changes in both parameters over the first 15 km (Fig. 3).

A. Luckman and others (unpublished information) find near-surface hyperbolic radar returns, indicative of surface crevasses along their radar transects, although they rarely observe them at the ice surface. Similarly, along our transect we also observe near-surface hyperbolic returns, although no surface crevasses were visually observed while conducting our radar surveys. We surmise that the surface crevasses are much narrower along our transect, as compared with the large surface crevasses observed proximally to Churchill Peninsula, and thus likely bridged by snow at the surface. Regardless, these observations provide evidence of widespread surface crevassing on the Larsen C ice shelf, although they may often be bridged at the surface and thus undetectable in both ground surveys and high-resolution (50 cm) satellite imagery.

Marine ice is believed to be an important component of the Larsen C ice shelf, particularly downstream of large promontories, where it likely sutures together neighboring flowbands while being advected to the calving front (Holland and others, 2009; Jansen and others, 2010). Holland and others (2009) suggest that the greatest rate of marine ice accumulation occurs in the wake of Churchill Peninsula, as the large-scale geostrophic-driven meltwater plume is forced out of the main Larsen C sub-ice-shelf cavity. Thus, this plume represents a large source of meltwater, which, due to its buoyant nature, may enter a basal crevasse, becoming supercooled as it rises in the water column before accreting as marine ice along the upper walls and at the apex of the crevasse (Khazendar and Jenkins, 2003). However, the return in the radar from the apex of the crevasse does not systematically differ along the length of the profile, which might be expected if the apexes were becoming filled with marine ice (Fig. 2). However, it is

unclear whether accreting marine ice would completely heal the crack, thus removing the sharp corner reflector and preventing a radar return from this point. Further, some studies suggest that even if the apex were filled with marine ice, the radar return would still originate at the meteoric/marine-ice interface due to the strong absorptive properties of the marine ice (Lambrecht and others, 2007; Holland and others, 2009). Therefore the radar data are inconclusive as to whether marine ice is being deposited within the basal crevasses, although considering the overall evolution in crevasse geometry along the transect, this process is likely.

An alternative process that could lead to a similar evolution in basal crevasse shape is a melt-driven convective cycle within the crevasse, as modeled by Khazendar and Jenkins (2003), that results in a widening of the base while depositing tens of meters of marine ice at the apex and along the upper walls. However, in this scenario, melting of the basal crevasse edges would lead to a rounding-off of the bottom corners and a gradual fading of the radar hyperbolas that originate from these once sharp corners. Thus, as the bottom hyperbolas remain strong along the length of the profile, we do not believe that basal melting is occurring in earnest. Further, this melt-driven convective cycle does not explain the formation of surface crevasses on the crests, and thus we suggest that the combination of bending stresses and possibly marine ice deposition, from a primarily distant meltwater source, is the more likely explanation for the observed evolution in basal crevasse geometry and surface crevasse formation.

Basal crevasses are inherently large-scale structural weaknesses within the ice shelf, that are further compounded by the fact that the ice-shelf surface lowers above these features to maintain hydrostatic equilibrium (Figs 2 and 4c). Surface depressions are likely locations for meltwater to accumulate, as observed in the Crane Glacier domain of the Larsen B ice shelf prior to its break-up (Glasser and Scambos, 2008). Larsen C does not currently support widespread surface melt ponds, despite extensive surface melt during the summer months. Shallow firn cores (~7 m) in the vicinity of the radar profile contain thick, refrozen meltwater layers, suggesting that the shelf surface is evolving towards the point where it will be able to support melt ponds in the future. Holland and others (2011) suggest 2–8 m of air content remains in the firn column along this transect, in contrast to ~20 m in the more southerly sectors of Larsen C. Thus, if the observed warming and subsequent increase in meltwater production continues along the AP, the northern sectors of Larsen C will likely support melt ponds in the near future. The hydrostatically adjusted surface troughs above the basal crevasses are likely locations for meltwater to pond, essentially creating small-scale catchment basins forming the requisite reservoirs for crevasse hydrofracture. This mechanism overcomes the necessity of very high ablation rates in order to produce enough meltwater to maintain surface crevasses at the critical threshold as they propagate further into the ice.

Surface crevasses, aligned along the crests and flanks of the surface undulations, are the result of an extensional bending stress induced by the presence of the basal crevasses and have important implications for ice-shelf stability. First, without surface crevasses, meltwater is stranded on the ice-shelf surface, with no means to propagate downwards. This is most clearly observed on the George VI Ice Shelf, which undergoes extensive surface

melt and ponding each summer, but is in compression between the peninsula and Alexander Island, and therefore lacks surface crevasses. This ice shelf has remained stable despite the abundant meltwater on the surface (Cook and Vaughan, 2010). In contrast, if the northern sector of Larsen C begins to support widespread melt ponds in the future, an extensive and well-developed surface crevasse network already exists to drain this meltwater. Second, if meltwater-driven hydrofracture does occur in the future, Larsen C would be much more likely to undergo a disintegration-style collapse, similar to Larsen A and B, than if the basal crevasses, with no surface crevasing, were to define future rifts. In this latter case, the dimensions of the subsequent icebergs would be stable (i.e. length (1200 m) \gg height (300 m)). However, the presence of surface crevasses would likely render the ice shelf into narrow elongate blocks, which are gravitationally unstable and would quickly overturn, further contributing to the disintegration event (MacAyeal and others, 2003).

Despite the simplified geometry of the model, it accurately predicts the height to which the basal crevasses will propagate using current-day parameters for Larsen C. Current observations of ice-shelf thinning and acceleration suggest that changes currently occurring on Larsen C will increase the overall stress intensity factor, allowing new basal crevasses to propagate further into the ice shelf. Rising atmospheric temperatures will oppose this increase, although there will be a substantial temporal lag for this forcing to equilibrate with the entire ice column. Thus, if the observed thinning and accelerating trends continue in the northern sector of Larsen C, it can be expected that new basal crevasses will propagate higher within the ice shelf.

CONCLUSION

We identify 27 basal crevasses along a 31 km transect on the northern sector of the Larsen C ice shelf. Widely spaced crevasses emerge from a region of multiple, shallow basal fractures and are found to initially penetrate to heights of ~130 m into the ice, the equivalent of ~40% of the ice thickness. The crevasses evolve along the length of the transect to become both shallower and broader features, most likely as a result of bending stresses and marine ice accretion in the crevasse apex. Application of the LEFM model accurately predicts the height to which the basal crevasses currently penetrate. Sensitivity studies of model parameters suggest that if the Larsen C ice shelf continues to accelerate and thin, basal crevasses that subsequently form will penetrate higher within the ice shelf. Basal crevasses will control the distribution of meltwater on the ice-shelf surface, resulting in ponds aligned with surface troughs. This creates the necessary reservoir for meltwater-driven crevasse hydrofracture and provides the initial surface crevasses, increasing the risk that full-thickness rifts will form where surface and basal crevasses intersect. This points to the need to better understand ice-shelf structure and the evolution of these features in a warming climate in order to understand and predict ice-shelf disintegration.

ACKNOWLEDGEMENTS

This work is funded by US National Science Foundation (NSF) Office of Polar Programs (OPP) research grant 0732946. The British Antarctic Survey provided exceptional

field support, without which this work would not have been possible. M. van den Broeke provided the firm correction and E. Rignot provided InSAR-derived surface velocities. Geospatial support for this work was supported by the Polar Geospatial Center under NSF OPP agreement ANT-1043681. We thank three anonymous reviewers and the scientific editor, Adrian Jenkins, who provided constructive feedback that substantially improved the paper.

REFERENCES

- Braun M, Humbert A and Moll A (2009) Changes of Wilkins Ice Shelf over the past 15 years and inferences on its stability. *Cryosphere*, **3**(1), 41–56
- Casassa G and Whillans IM (1994) Decay of surface topography on the Ross Ice Shelf, Antarctica. *Ann. Glaciol.*, **20**, 249–253
- Cook AJ and Vaughan DG (2010) Overview of areal changes of the ice shelves on the Antarctic Peninsula over the past 50 years. *Cryosphere*, **4**(1), 77–98
- Das SB and 6 others (2008) Fracture propagation to the base of the Greenland Ice Sheet during supraglacial lake drainage. *Science*, **320**(5877), 778–781
- Fahnestock MA, Abdalati W and Shuman CA (2002) Long melt seasons on ice shelves of the Antarctic Peninsula: an analysis using satellite-based microwave emission measurements. *Ann. Glaciol.*, **34**, 127–133
- Fahrbach E, Hoppema M, Rohardt G, Schröder M and Wisotzki A (2004) Decadal-scale variations of water mass properties in the deep Weddell Sea. *Ocean Dyn.*, **54**(1), 77–91
- Förste C and 12 others (2008) The GeoForschungsZentrum Potsdam/Groupe de Recherche de Géodésie Spatiale satellite-only and combined gravity field models: EIGEN-GL04S1 and EIGEN-GL04C. *J. Geod.*, **82**(6), 331–346
- Glasser NF and Scambos TA (2008) A structural glaciological analysis of the 2002 Larsen B ice-shelf collapse. *J. Glaciol.*, **54**(184), 3–16
- Glasser N and 7 others (2009) Surface structure and stability of the Larsen C ice shelf, Antarctic Peninsula. *J. Glaciol.*, **55**(191), 400–410
- Griggs JA and Bamber JL (2009) Ice shelf thickness over Larsen C, Antarctica, derived from satellite altimetry. *Geophys. Res. Lett.*, **36**(19), L19501 (doi: 10.1029/2009GL039527)
- Haran T, Bohlander J, Scambos T, Painter T and Fahnestock M (2006) *MODIS mosaic of Antarctica (MOA) image map*. National Snow and Ice Data Center, Boulder, CO. Digital media
- Holland PR, Corr HFJ, Vaughan DG, Jenkins A and Skvarca P (2009) Marine ice in Larsen Ice Shelf. *Geophys. Res. Lett.*, **36**(11), L11604 (doi: 10.1029/2009GL038162)
- Holland PR and 6 others (2011) The air content of Larsen Ice Shelf. *Geophys. Res. Lett.*, **38**(10), L10503 (doi: 10.1029/2011GL047245)
- Jacobs SS, Jenkins A, Giulivi CF and Dutriex P (2011) Stronger ocean circulation and increased melting under Pine Island Glacier ice shelf. *Nature Geosci.*, **4**(8), 519–523
- Jansen D, Kulesa B, Sammonds PR, Luckman A, King EC and Glasser NF (2010) Present stability of the Larsen C ice shelf, Antarctic Peninsula. *J. Glaciol.*, **56**(198), 593–600
- Jenkins A, Corr HFJ, Nicholls KW, Stewart CL and Doake CSM (2006) Interactions between ice and ocean observed with phase-sensitive radar near an Antarctic ice-shelf grounding line. *J. Glaciol.*, **52**(178), 325–346
- Jezek KC (1984) A modified theory of bottom crevasses used as a means for measuring the buttressing effect of ice shelves on inland ice sheets. *J. Geophys. Res.*, **89**(B3), 1925–1931
- Jezek KC, Bentley CR and Clough JW (1979) Electromagnetic sounding of bottom crevasses on the Ross Ice Shelf, Antarctica. *J. Glaciol.*, **24**(90), 321–330
- Johnston TL and Parker ER (1957) *Preliminary investigation of surface effects in flow and fracture*. Minerals Research Laboratory, Institute of Engineering Research, University of California, Berkeley, CA (Tech. Rep. 27(16))
- Khazendar A and Jenkins A (2003) A model of marine ice formation within Antarctic ice shelf rifts. *J. Geophys. Res.*, **108**(C7), 3235 (doi: 10.1029/2002JC001673)
- Khazendar A, Rignot E and Larour E (2011) Acceleration and spatial rheology of Larsen C Ice Shelf, Antarctic Peninsula. *Geophys. Res. Lett.*, **38**(9), L09502 (doi: 10.1029/2011GL046775)
- Lambrech A, Sandhager H, Vaughan DG and Mayer C (2007) New ice thickness maps of Filchner–Ronne Ice Shelf, Antarctica, with specific focus on grounding lines and marine ice. *Antarct. Sci.*, **19**(4), 521–532
- MacAyeal DR, Scambos TA, Hulbe CL and Fahnestock MA (2003) Catastrophic ice-shelf break-up by an ice-shelf-fragment-capsize mechanism. *J. Glaciol.*, **49**(164), 22–36
- Nicholls KW, Pudsey CJ and Morris P (2004) Summertime water masses off the northern Larsen C Ice Shelf. *Geophys. Res. Lett.*, **31**(9), L09309 (doi: 10.1029/2004GL019924)
- Orheim O (1982) Radio echo-sounding of Riiser-Larsenisen. *Ann. Glaciol.*, **3**, 355
- Orr A and 6 others (2004) A ‘low-level’ explanation for the recent large warming trend over the western Antarctic Peninsula involving blocked winds and changes in zonal circulation. *Geophys. Res. Lett.*, **31**(6), L06204 (doi: 10.1029/2003GL019160)
- Orr A and 7 others (2008) Characteristics of summer airflow over the Antarctic Peninsula in response to recent strengthening of westerly circumpolar winds. *J. Atmos. Sci.*, **65**(4), 1396–1413
- Padman L, Fricker HA, Coleman R, Howard S and Erofeeva L (2002) A new tide model for the Antarctic ice shelves and seas. *Ann. Glaciol.*, **34**, 247–254
- Rist MA (1996) Fracture mechanics of ice shelves. *FRISP Rep.* 10, 102–105
- Rist MA, Sammonds PR, Murrell SAF, Meredith PG, Oerter H and Doake CSM (1996) Experimental fracture and mechanical properties of Antarctic ice: preliminary results. *Ann. Glaciol.*, **23**, 284–292
- Rist MA, Sammonds PR, Oerter H and Doake CSM (2002) Fracture of Antarctic shelf ice. *J. Geophys. Res.*, **107**(B1) (doi: 10.1029/2000JB000058)
- Robertson R, Visbeck M, Gordon AL and Fahrbach E (2002) Long-term temperature trends in the deep waters of the Weddell Sea. *Deep-Sea Res. II*, **49**(21), 4791–4806
- Sandhäger H, Rack W and Jansen D (2005) Model investigations of Larsen B Ice Shelf dynamics prior to the breakup. *FRISP Rep.* 16, 5–12
- Scambos TA, Hulbe C, Fahnestock M and Bohlander J (2000) The link between climate warming and break-up of ice shelves in the Antarctic Peninsula. *J. Glaciol.*, **46**(154), 516–530
- Scambos T, Hulbe C and Fahnestock M (2003) Climate-induced ice shelf disintegration in the Antarctic Peninsula. In Domack EW, Burnett A, Leventer A, Conley P, Kirby M and Bindschadler R eds. *Antarctic Peninsula climate variability: a historical and paleoenvironmental perspective*. American Geophysical Union, Washington, DC, 79–92 (Antarctic Research Series 79)
- Scambos T and 7 others (2009) Ice shelf disintegration by plate bending and hydro-fracture: satellite observations and model results of the 2008 Wilkins ice shelf break-ups. *Earth Planet. Sci. Lett.*, **280**(1–4), 51–60
- Shepherd A, Wingham D, Payne T and Skvarca P (2003) Larsen ice shelf has progressively thinned. *Science*, **302**(5646), 856–859
- Swithinbank C (1977) Glaciological research in the Antarctic Peninsula. *Philos. Trans. R. Soc. London, Ser. B*, **279**(963), 161–183
- Van den Broeke M (2005) Strong surface melting preceded collapse of Antarctic Peninsula ice shelf. *Geophys. Res. Lett.*, **32**(12), L12815 (doi: 10.1029/2005GL023247)

- Van der Veen CJ (1998a) Fracture mechanics approach to penetration of surface crevasses on glaciers. *Cold Reg. Sci. Technol.*, **27**(1), 31–47
- Van der Veen CJ (1998b) Fracture mechanics approach to penetration of bottom crevasses on glaciers. *Cold Reg. Sci. Technol.*, **27**(3), 213–223
- Van der Veen CJ and Whillans IM (1989) Force budget: I. Theory and numerical methods. *J. Glaciol.*, **35**(119), 53–60
- Vaughan D (2006) Recent trends in melting conditions on the Antarctic Peninsula and their implications for ice-sheet mass balance and sea level. *Arct. Antarct. Alp. Res.*, **38**(1), 147–152
- Vaughan DG and 8 others (2003) Recent rapid regional climate warming on the Antarctic Peninsula. *Climatic Change*, **60**(3), 243–274
- Weertman J (1973) Can a water-filled crevasse reach the bottom surface of a glacier? *IASH Publ.* 95 (Symposium at Cambridge 1969 – *Hydrology of Glaciers*), 139–145.
- Weertman J (1980) Bottom crevasses. *J. Glaciol.*, **25**(91), 185–188
- Zwally HJ, Abdalati W, Herring T, Larson K, Saba J and Steffen K (2002) Surface melt-induced acceleration of Greenland ice-sheet flow. *Science*, **297**(5579), 218–222